

# Derivation of a Reference Shear-Wave Velocity Model from Empirical Site Amplification

by Valerio Poggi, Benjamin Edwards, and Donat Fäh

**Abstract** The definition of a reference bedrock condition representative of a region of interest is of great significance in seismic-hazard assessment. It is highly beneficial when ground-motion prediction equations are referenced to a specific site condition, particularly in the case of site-specific seismic-hazard analyses. When known, the effect of any given site with respect to the reference can then be applied to the predicted ground motion. However, the choice of a reference velocity profile is not straightforward, mainly due to the high variability of the velocity structure in the shallower layers.

A new method to define the regional reference rock profile is proposed. The method relates quarter-wavelength average velocity at a site to frequency-dependent amplification. A reference bedrock velocity profile can then be directly defined in relation to expected amplification characteristics over a number of sites. We compare 27 quarter-wavelength velocity profiles from seismic station locations in Switzerland with empirical amplification functions derived from spectral modeling. From this comparison, a set of frequency-dependent calibration relationships is established. Assuming that the reference profile is defined by a lack of any relative amplification, the quarter-wavelength velocity profile that corresponds to unitary spectral amplification can be extracted. The reference velocity profile can then be obtained through an inversion procedure and defines the reference for the ground-motion prediction equation (GMPE).

The proposed reference velocity profile is compared with previous reference velocity profiles. A good agreement is found between the different methods. Additionally, an estimation of the transfer function for the Swiss reference rock condition is provided. This can be used to correct recorded or estimated spectral amplitudes for the local response of the reference site. Finally, it is shown that the coefficients from the aforementioned correlations can be used to estimate a generic amplification function at any site with a known quarter-wavelength velocity profile.

## Introduction

It is well known that local site conditions can strongly influence the amplitude and duration of ground motion during an earthquake (e.g., Bard *et al.*, 1988; Aki, 1993). In particular, soft sediments with low seismic velocities with respect to the underlying bedrock can lead to large amplification of ground motion at the surface (e.g., Bonilla *et al.*, 1997; Pratt *et al.*, 2003). In site-specific probabilistic seismic-hazard assessment (PSHA), predicted ground motion must be referenced to a specific site condition so it can subsequently be corrected with reference to the site of interest (Kawase, 2006). The use of an incorrect reference condition for a ground-motion prediction equation (GMPE) may lead to an over- or underestimation of the final computed seismic hazard (Steidl *et al.*, 1996).

The correction for, or application of, site amplification is usually performed through a deconvolution or convolution of earthquake recordings with a soil response function. This can be done in either the time or frequency domain. The latter is the most common approach. Site amplification can be computed analytically (e.g., Abbiss, 1989), if sufficient knowledge of the velocity structure is available, or measured, for example by using site-to-reference spectral ratios (e.g., Borchardt, 1970; Borchardt and Gibbs, 1976). Correcting for the site amplification, however, always relies on the definition of a reference velocity profile, for which amplification phenomena are well known. The choice of a common reference is not always straightforward. Over small areas, the average characteristics of the rock basement can be used,

and the reference can be defined based on direct geological or geophysical knowledge (e.g., Romero and Rix, 2001). Over large areas, however, the selection might be more problematic. In such a case, due to the large variability of ground conditions, more general criteria of selection are necessary (Yu and Haines, 2003).

Reference rock conditions have previously been defined using simplified site geology classes or by directly estimating average velocities for the upper few tens of meters (e.g., National Earthquake Hazards Reduction Program [NEHRP] [BSSC, 2001], EuroCode 8 [EC8] [CEN, 2004]). The main disadvantage of using such approaches is the lack of a clear physical justification as to how the reference conditions are selected. In some cases, the reference is extrapolated beyond the depths directly measured using regional models (Douglas *et al.*, 2009), for example, those computed using travel-time seismic tomography. This is partially correct because tomographic models are sufficiently accurate at depth (i.e., of the order kilometers), but the interpolation between the uppermost velocity (e.g.,  $V_{S30}$ ) and the velocity at depth is rather arbitrary. Local amplification, however, strongly depends on the velocity contrasts within the shallower layers. Several attempts have been made to improve the accuracy of the reference profiles at shallow depths, for example, through the use of simplified gradient models (Boore and Joyner, 1997). However, the choice of the correct parametrization to constrain these models still remains an open issue.

An alternative method to retrieving the reference velocity profile for hazard computation is proposed. Our approach focuses on the definition of a reliable way to constrain the first few hundred meters of the reference model. The method is based on the comparison of average velocities at specific seismic station locations with the corresponding amplification obtained from spectral modeling (e.g., Edwards *et al.*, 2008; Drouet, Chevrot, *et al.*, 2008). To relate the frequency-dependent amplification functions to the velocity information, the quarter-wavelength approximation (Joyner *et al.*, 1981) is used. The advantage of such a procedure is the possibility of relating the depth over which the average velocity will be computed to a specific wavelength. As such, all average velocity estimates (versus depth) will be uniquely associated to a specific amplification factor at a defined frequency.

From the ensemble of measurement locations (Fig. 1), amplification versus average velocity relationships were computed for a set of discrete frequencies between 1 and 15 Hz. From these relations, the quarter-wavelength average velocities corresponding to unitary amplification were extracted and collected. In this way, a quarter-wavelength representation of the reference velocity profile is established. However, for site characterization, a representation of the shear-wave velocity profile versus depth is required. This is subsequently obtained through an inversion procedure. As a last step, a reference *SH*-wave amplification function

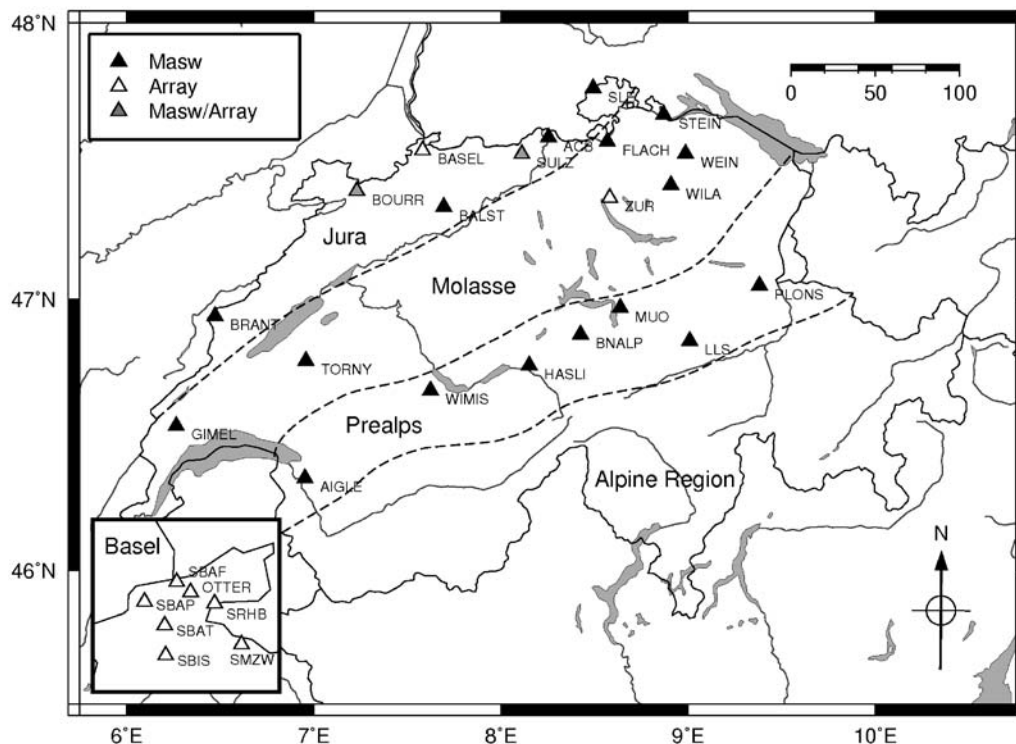


**Figure 1.** Location of the 27 seismic stations investigated during the PEGASOS Refinement Project. Of these stations, 17 were characterized using an active MASW technique, 8 using array analysis of ambient noise recordings, and stations BOURR and SULZ with both the techniques. The stations shown are part of the SDSNet and the SSMNet. The approximate limits between main geological domains are shown.

was computed from the retrieved velocity profile to correct to the source condition. This transfer function can then be used as part of a stochastic model (e.g., Boore, 2003; Atkinson and Boore, 2006), which will simulate ground motion at the reference profile, given a defined source and the attenuation characteristics of the propagation medium.

As an additional outcome, we show how the generic amplification function at a site with known quarter-wavelength average velocity can be estimated using the coefficients from the frequency-dependent correlations. The comparison between the reconstructed amplification and theoretical one-dimensional (1D) amplification models at test sites are consistent with observed amplification.

### Selection of $V_S$ Velocity Profiles for Specific Station Locations

Twenty seismic stations of the Swiss Digital Seismic Network (SDSNet, Baer *et al.*, 2007) and the Swiss Strong Motion Network (SSMNet) have been investigated within the PEGASOS Refinement Project (PRP; Fäh *et al.*, 2009). The PRP is a seismic-hazard assessment project coordinated by *swissnuclear* (Renault *et al.*, 2010). The locations of the investigated sites were defined in order to sample the most typical rock site conditions of the Swiss Alpine Foreland (Figure 1). Seven additional stations were investigated during a previous microzonation study (Havenith *et al.*, 2007). In particular, of the total 27 investigated sites, 7 were selected in the Molasse Basin (GIMEL, TORN, ZUR, WILA, WEIN, FLACH, and STEIN), 7 were spread along the northern flank of the Alpine chain (AIGLE, WIMIS, HASLI, BNALP, MUO, LLS, and PLONS), and 13 in the Jura region. Of these last, 7 stations (OTTER, SBAF, SBAP, SBAT, SBIS, SMZW, and SRHB) are located inside the city of Basel, while the remaining 6 are distributed along the Jura chain (BRANT, BOURR, BALST, SULZ, ACB, and SLE). For all these sites a large number of recordings exist, which are used to derive the empirical site amplification terms.

The main target of the PRP investigations was the characterization of the first 50 to 100 m of the ground beneath each selected station. However, not all the stations were equally accessible for surveying. In some cases (e.g., sensors located in tunnels or on steep topography) the measurement point did not match the sensor location. In such situations some corrections were therefore necessary. For example, the removal of the upper few meters of soft sediments from the measured profiles in order to account for a buried sensor at the station (Fäh *et al.*, 2009).

In order to obtain the shear-wave velocity profiles, nonintrusive active and passive seismic techniques, such as multichannel analysis of surface waves (MASW) and high-resolution  $f$ - $k$  analysis (HRFK), were applied. The MASW method (Park *et al.*, 1999) is based on the analysis of the dispersion characteristics of surface waves (specifically Rayleigh waves), which are artificially generated by an active source located at the surface. The main advantage in using

such a technique is the possibility of obtaining reliable estimations of the local velocity structure in a fast and cost-effective way. Consequently, large areas can be covered by a single survey. For each location where MASW was applied, several velocity profiles were provided along sections of about 50 m in length. In order to facilitate the interpretation,  $P$ - and  $S$ -wave seismic investigations were also carried out along the same profile (GeoExpert AG, 2009, technical report). From selected portions of these sections, mean 1D velocity profiles were then calculated (Figure 2). This approach gave us the possibility of accounting for the local variability of the soil conditions and producing statistics on the final results. The main limitation of the MASW technique, however, is its low resolution at large depths. The resolution is controlled by the frequency band and the energy of the active source employed (in this case a sledgehammer).

The HRFK is an array technique for surface-wave analysis, originally proposed by Capon (1969) and subsequently optimized by Fäh *et al.* (2008) and Poggi and Fäh (2009) to analyze the full-ground motion (both Love and Rayleigh waves) from one- or three-component recordings of ambient noise. Unlike MASW, the use of passive-natural microvibration allows the investigation of greater depths (Yamanaka *et al.*, 1994) but conversely yields limited resolution in the last few upper meters. This limitation is mainly due to the small number of receivers usually employed during a survey but also to the moderate energy content of the ambient vibration wave field at high frequencies. This kind of survey produces a single 1D velocity profile as output, which is representative of the average conditions over the whole area covered by the array. It is possible to define uncertainties on the measured velocity profile if the uncertainties of the surface wave dispersion information are extended to the inverted velocity profile.

Of the 27 selected station locations, 10 were investigated using HRFK analysis (all Basel stations, plus ZUR, SULZ, and BOURR), while 19 were investigated using MASW. Only stations BOURR and SULZ were surveyed using both techniques in order to verify the consistency of the results.

### The Quarter-Wavelength Velocity Approximation

The quarter-wavelength approximation was initially proposed by Joyner *et al.* (1981) and subsequently optimized by Boore (2003) to compute amplification factors for generic rock profiles. The method is based on the estimation of the average seismic parameters (velocity and density) up to a depth that corresponds to one quarter of the wavelength of interest. For a specific frequency, amplification factors can then be computed as the square root of the impedance ratio between average depth and reference.

The physical justification of using  $1/4$  of the wavelength of interest as the averaging depth is that, in the simplified 1D case (with one layer over a homogeneous half-space), a maximum in  $SH$ -wave amplification is observed at a defined

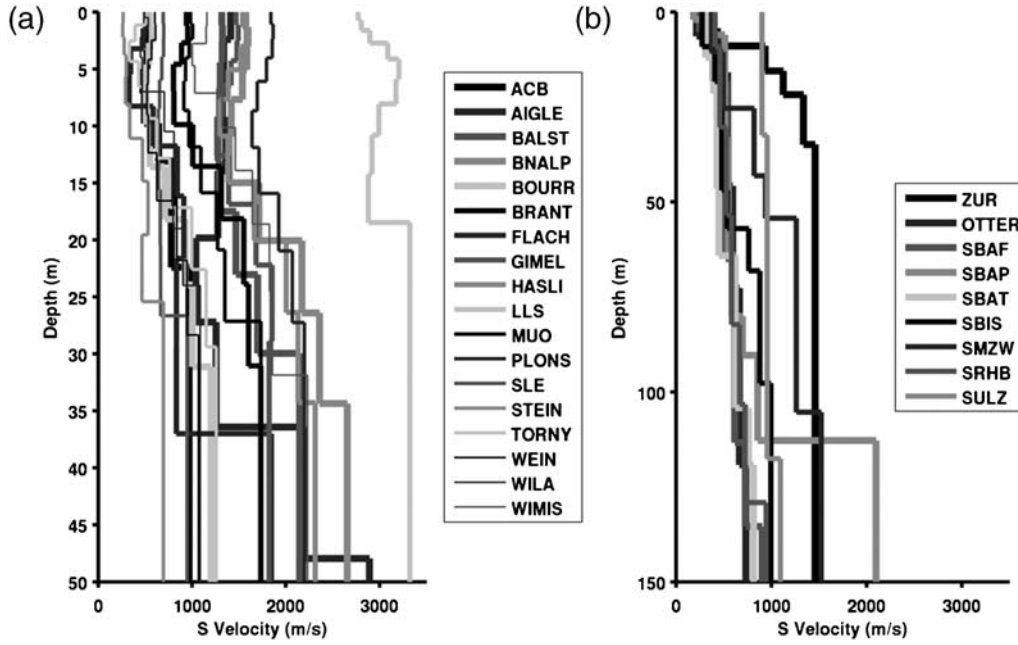


**Figure 2.** Velocity profiles from the 27 selected seismic station locations in Switzerland. Each velocity profile has been obtained from the inversion of surface wave dispersion (from (a) active MASW and (b) passive array  $f$ - $k$  analysis) and extrapolated beyond the resolution of the measurements.

frequency, the fundamental frequency of resonance  $f_0^{SH}$ , which corresponds to this expression (Roesset, 1970):

$$f_0^{SH} = \frac{V_{S_{\text{Layer}}}}{4 \cdot z_{\text{Layer}}}, \quad (1)$$

where  $V_{S_{\text{Layer}}}$  and  $z_{\text{Layer}}$  are the shear-wave velocity and thickness of the layer, respectively. Conversely, given any frequency, the largest amplification will occur at a specific layer depth corresponding to 1/4 of the wavelength of resonance  $\lambda_0^{SH}$ :

$$z_{\text{Layer}} = \frac{V_{S_{\text{Layer}}}}{4 \cdot f_0^{SH}} = \frac{\lambda_0^{SH}}{4}. \quad (2)$$

Following this, the quarter-wavelength method assumes that, at any given frequency  $f$ , a vertically heterogeneous soil profile can be seismically characterized by its average velocity computed down to a depth  $z(f)$  corresponding to 1/4 of the wavelength of interest. The quarter-wavelength velocity ( $V_S^{\text{QWL}}$ ) can then be obtained for a specific frequency by travel-time averaging over the input profile through the minimization of

$$\arg \min_{z(f)} \left\{ z(f) - \frac{V_S^{\text{QWL}}[z(f)]}{4f} \right\}, \quad (3)$$

given that

$$V_S^{\text{QWL}}[z(f)] = z(f) \left[ \int_0^{z(f)} \frac{1}{V_S[z(f)]} dz(f) \right]^{-1}. \quad (4)$$

This is achieved through a direct search approach over  $z$  in order to recursively converge at the solution of the minimi-

zation problem. Upon obtaining  $z(f)$ , the average quarter-wavelength density  $\rho^{\text{QWL}}[z(f)]$  can also be computed:

$$\rho^{\text{QWL}}[z(f)] = \frac{1}{z(f)} \left\{ \int_0^{z(f)} \rho[z(f)] dz(f) \right\}. \quad (5)$$

To compute the final amplification, however, the quarter-wavelength method does not rely on the computation of the  $SH$ -wave transfer function. To avoid the inclusion of the characteristic resonance peaks (from the interference of up- and downgoing reflected waves), the amplification is calculated as the square root of the ratio between the seismic impedance from the quarter-wavelength approximation and that of the source reference (generally the bedrock in the case of sedimentary basins):

$$A[z(f)] = \sqrt{\frac{\rho^c V_S^c}{\rho^{\text{QWL}}[z(f)] V_S^{\text{QWL}}[z(f)]}}. \quad (6)$$

This approach always results in a smoothed amplification function. The quarter-wavelength method might therefore be advantageous because in most cases these resonance amplification maxima result only as consequence of the discretization of the velocity profile for modeling. Following this procedure, then, quarter-wavelength curves were calculated from the ensemble of all available velocity profiles at each station location. For each data set, finally, the mean value and standard deviation at discrete frequencies of 1 to 15 Hz were computed (Figure 3).

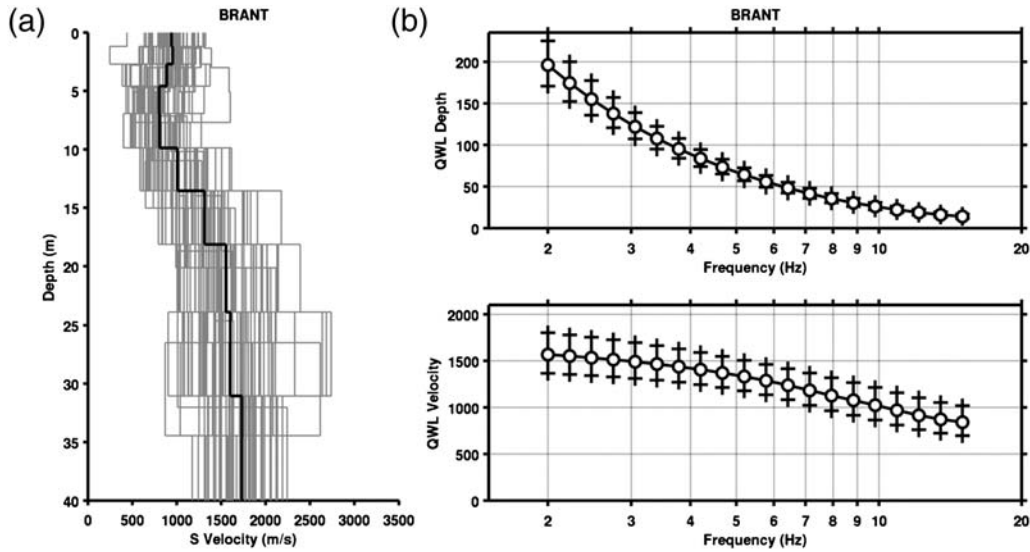


**Figure 3.** (a) Example of measured  $V_S$  velocity profiles at the station BRANT and (b) its quarter-wavelength representation. Statistics are computed over the ensemble of all inverted velocity profiles from surface-wave analysis.

### Obtaining Site-Specific Amplification

The problem of separating source, path, and site effects in terms of physical phenomena is a nontrivial and nonlinear problem (e.g., Scherbaum, 1990). While the problem can be simplified in a way similar to that commonly used in engineering applications (e.g., Akkar and Bommer, 2007), such that the problem is linear, it is our opinion that the interpretation of such a model is more difficult to justify in a physical sense.

The Brune (1970, 1971) source model has been frequently shown to be a powerful way of modeling the far-field spectra of small earthquakes (Anderson and Hough, 1984; Boore, 1983; 2003; Hanks and McGuire, 1981). In fact, Randall (1973) found that the Brune far-field model can be used to describe observed far-field earthquake spectra even in the case where the exact method of dislocation is unknown. The Brune (1970, 1971) source model is therefore commonly used in the deconvolution of source, site, and path effects for small to moderate earthquakes and the simulation of ground motion in regions of low to moderate seismicity (e.g., Atkinson and Boore, 2006).

An initial fit of the Brune (1970, 1971) source to each event, allowing for path variable attenuation and source-specific stress drop is performed following a modification of the spectral deconvolution procedure presented in Edwards *et al.* (2008) and Edwards and Rietbrock (2009). We adopt this model such that site-specific amplification functions can be obtained through a combination of residual analysis and direct inversion of numerous earthquake recordings. As a consequence of the model formulation, the amplification terms derived from this spectral fitting method are referenced to an unknown condition that represents the refer-

ence rock profile. Previous work by Drouet, Triantafyllidis, *et al.* (2008) showed that amplification functions derived following the spectral deconvolution approach were consistent with site-to-reference spectral ratios. Furthermore, we later show that the amplification functions derived using this approach are consistent with theoretical *SH*-amplification functions derived from measured  $V_S$  profiles.

It is assumed that the Fourier velocity spectrum,  $\Omega_{ij}(f, r)$ , observed at a recording station,  $j$ , originating from an earthquake,  $i$ , can be represented as

$$\Omega_{ij}(f, r) = 2\pi f E_i(f, f_{ci}) B_{ij}(f, t_{ij}^*) S_{ij}(r, r_{0\dots n-1}, \lambda_{1\dots n}) T_j(A_j, f, \kappa_j) I_j(f), \quad (7)$$

where  $f$  is the frequency;  $r$  is the hypocentral distance;  $E_i(f, f_{ci})$  is the source model (the far-field displacement spectrum);  $B_{ij}(f, t_{ij}^*)$  is the attenuation along the ray path;  $S_{ij}(r, r_{0\dots n-1}, \lambda_{1\dots n})$  is the frequency-independent amplitude decay with distance;  $T_j(A_j, f, \kappa_j)$  is the site amplification function at the station; and  $I_j(f)$  is the instrument response function.

The source spectrum is modeled by

$$E_i(f, f_{ci}) = \Psi_{0i} \frac{1}{[1 + (\frac{f}{f_{ci}})^2]}, \quad (8)$$

(Brune 1970, 1971), where  $\Psi_{0i}$  is the long-period plateau value at the source, and  $f_{ci}$  is the source corner frequency. Assuming whole-path attenuation, the attenuation along the path of propagation is

$$B_{ij}(f, t_{ij}^*) = e^{(-\pi f \frac{\tau_{ij}}{Q_{0ij}})} = e^{(-\pi f t_{ij}^*)}, \quad (9)$$

where  $\tau_{ij}$  is the travel time;  $Q_{0ij}$  is the dimensionless quality factor (e.g., Rietbrock, 2001); and  $t_{ij}^*$  is the whole-path attenuation operator. We choose to model frequency-independent  $Q$ , as the frequency dependence of  $Q$  is difficult to derive and may introduce further trade-offs. For instance, Drouet *et al.* (2010) show that there are negligible differences in the residual misfit to data recorded in France for eight independently derived  $Q$  models (with  $Q(f) = Q_0 f^\alpha$ ) with frequency dependence ranging between  $\alpha = 0$  and 1.1. In fact,  $Q$  is well known to trade off with other parameters in spectral deconvolution methods. However, it is important to note that we are interested in this case in relative variations at individual stations. On average, and by definition, the inversion residuals are flat over the ensemble of recordings at all stations. It is only site-specific variations that are later extracted for analysis. Therefore, regardless of what we choose to predefine (e.g., frequency dependence of  $Q$ ), other parameters (such as the source corner frequency) may accommodate the changes due to trade-offs and may result in flat residuals over the ensemble of recordings. However, site-to-site variations extracted from the residuals will be relatively unaffected by this trade-off due to the averaging over many earthquakes, distances, and depths.

The apparent geometrical spreading function, which may include factors such as phase interference and dispersion, focusing or defocusing, and scattering (e.g., Atkinson and Mereu, 1992), is described by a piecewise function comprising segments of constant exponential decay:

$$S_{ij}(r, r_{0\dots n-1}, \lambda_{1\dots n}) = \left\{ \begin{array}{ll} \left(\frac{1}{r}\right)^{\lambda_1} & r \leq r_1 \\ S(r_1) \left(\frac{r_1}{r}\right)^{\lambda_2} & r_1 \leq r \leq r_2 \\ \dots & \dots \\ S(r_n) \left(\frac{r_n}{r}\right)^{\lambda_n} & r \geq r_n \end{array} \right\}. \quad (10)$$

Finally, the local site transfer function is given by

$$T_j(A_j, f, \kappa_j) = A_j a_j(f) e^{(-\pi f \kappa_j)}, \quad (11)$$

where  $A_j$  is the average site amplification relative to the unknown reference rock profile (the average amplification over all frequencies);  $\kappa_j$  is a constant, site-related attenuation operator (e.g., Anderson and Hough, 1984); and  $a_j(f)$  is the frequency-dependent site amplification function. The data are carefully corrected for instrument response such that  $I_j(f) = 1.0$ .

The deconvolution of the model parameters is therefore solved in a two-stage approach. First, the frequency-dependent model components are obtained: a component describing the source model, controlled by  $f_{ci}$ ; the path attenuation, controlled by  $t_{ij}^* + \kappa_j$ ; and the normalized site amplification  $a_j(f)$ , along with a combined amplitude parameter, the signal moment:

$$\hat{\Omega}_{ij} = \Psi_{0i} A_j S_{ij}(r, r_{0\dots n-1}, \lambda_{1\dots n}). \quad (12)$$

The following minimization function is used:

$$\xi = \sum_{f=f_{\text{start}}}^{f_{\text{end}}} \frac{\{\log[\Omega_{ij}^o(f)] - \log[\Omega_{ij}^m(f)]\}}{f}, \quad (13)$$

where  $o$  refers to the observed data and  $m$  the modeled data. The use of  $1/f$  down-weights the higher frequency content of the spectra in favor of fitting the low-frequency plateau and source corner frequency. This is a subjective choice made in order to reduce the influence of more numerous high-frequency data and is similar to transforming the parameter space into the log-log domain (e.g., Ide *et al.*, 2003). A grid search around  $f_{ci}$  is performed with a Powell's minimization (Press *et al.*, 1997) of equation (13) to find  $t_{ij}^* + \kappa_j$  and the signal moment. Using the minimum misfit model, the factorial residuals, given by

$$\theta_{ij}(f) = \frac{\Omega_{ij}^o(f, r)}{\Omega_{ij}^m(f, r)}, \quad (14)$$

can then be used to reconstruct the frequency-dependent site function by taking the log-space mean of the factorial residuals at discrete frequencies over all events ( $i = 1, 2, 3 \dots n$ ) at a specific station,  $j$ :

$$\log[a_j(f)] = \frac{1}{N} \left\{ \sum_{i=1}^n \log[\theta_{ij}(f)] \right\}. \quad (15)$$

The signal moments are used in a second stage to separate the frequency-independent parameters  $\Psi_{0i}$ ,  $A_j$ , and  $S_{ij}(r, r_{0\dots n-1}, \lambda_{1\dots n})$ . The geometrical spreading term  $S_{ij}(r, r_{0\dots n-1}, \lambda_{1\dots n})$  is assumed to be consistent with initial spherical decay followed by trapped surface-wave (cylindrical) spreading after 150 km from the source:  $r_0 = 1$  km,  $r_1 = 150$  km;  $\lambda_1 = 1.0$  and  $\lambda_2 = 0.5$ . The signal moments can be expressed as a sum by taking the logarithm of equation (12):

$$\log(\hat{\Omega}_{ij}) = \log(\Psi_{0i}) + \log(A_j) + \log[S_{ij}(r, r_{0\dots n-1}, \lambda_{1\dots n})], \quad (16)$$

which can be solved using a least-squares (L2) minimization with a singular value decomposition (SVD) algorithm (Press *et al.*, 1997; Pozo, 2004). The inversion is constrained by assuming

$$\sum_{j=1}^j \log(A_j) = 0, \quad (17)$$

such that the parameter  $A_j$  is defined as an amplification relative to the reference rock. Data constraints are applied to prevent poorly determined parameters: The number of observations of one event and the overall number of observations at a station must both be greater than or equal to 10. In reality the number of recordings at the stations used in this study ranged from 13 to 360.

In order to assess whether the assumption that the geometrical decay can be described by spherical (followed by cylindrical) spreading, as defined by equation (10), we first compute the residual misfit of the far-field long-period plateau of the spectra ( $\hat{\Omega}_{ij}$ ). In this preliminary test, we invert for the long-period plateau of the spectra while accounting for this simple geometrical decay function, but without the use of site terms ( $A_j$ ). The resultant misfit is shown in Figure 4. On average there are no significant trends apparent with distance. We therefore use this decay function when inverting for the site terms ( $A_j$ ) in order to avoid any trade-off between the parameters.

In this application the site terms  $\bar{T}_j(A_j, f)$  were required, independent of attenuation, so they were reconstructed from  $A_j$  and  $a_j(f)$ , such that

$$\bar{T}_j(A_j, f) = A_j a_j(f), \quad (18)$$

(e.g., Figure 5). The uncertainty was propagated into  $\bar{T}_j(A_j, f)$  from  $A_j$  and  $a_j(f)$ . The 17,300 records (including both horizontal components) from 585 earthquakes occurring in Switzerland with  $M_L > 2.0$  were used to define the  $\bar{T}_j(A_j, f)$  for 77 sites in Switzerland, including the 27 used in this study (Edwards *et al.*, 2009). The multitaper algorithms (Lees and Park, 1995; Park *et al.*, 1987) with  $5 - 3\pi$  prolate tapers were used to compute the Fourier spectra of the combined  $S$  wave and coda of these earthquakes. The analysis window was defined following the method proposed by Raof *et al.*, (1999) to encapsulate 5% to 75% of the cumulative squared velocity of the record (a measure of significant shaking). A noise window is chosen to be as long as possible in order to enable the correct recovery of any long-period noise. It starts at the beginning of the trace and continues over a duration equal to 75% of the time until the  $P$ -wave arrival. This also ensures that potentially inaccurate  $P$ -wave arrival time picks (or estimates) do not lead to the noise win-

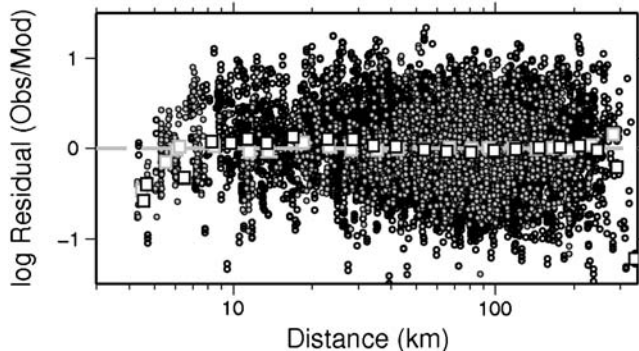


**Figure 4.** Residual misfit of  $\hat{\Omega}_{ij}$  (the far-field long-period displacement plateau) for magnitudes greater than 3 and distances greater than 10 km after being fit with the geometrical decay function described by equation (10) and  $r_0 = 1$  km,  $r_1 = 150$  km;  $\lambda_1 = 1.0$  and  $\lambda_2 = 0.5$ . The gray symbols are from events occurring in the Swiss foreland. The black symbols are from events occurring in the Swiss Alps. The squares indicate average residual at a given hypocentral distance.

dow being contaminated by the  $P$ -arrival. A signal-to-noise ratio of over three was then required to include the data in the inversion.

In a future stage of our research, we plan to free more of the parameters of the spectral modeling in order to assess the robustness of the results. One possibility is to follow a two-step nonparametric generalized inversion as proposed by Castro *et al.* (1990) and used by other authors, for example, Parolai *et al.* (2004); or Bindi *et al.* (2006). This might help in reducing the number of assumptions used to constrain the inversion procedure; for example, we could use  $1/R$  geometrical spreading, or we could model attenuation using a simple exponential function.

### Quarter-Wavelength Velocity Classes Versus Predicted Amplification

At each station location, quarter-wavelength velocity curves were correlated with the estimated amplification functions from the spectral modeling approach. The correlation was made over a set of discrete frequencies in the range between 1 and 15 Hz. The choice of using 1 Hz as the lowest resolvable frequency for the computation comes from the fact that the velocity profiles from both MASW and array analysis are optimistically reliable only down to a depth range between 50 and 150 m. This limitation can be partially overcome by the smoothing effect of the quarter-wavelength representation and by introducing some a priori constraint, such as forcing the extended profile to have a gradient. However, including frequencies lower than 1 Hz might lead to erroneous results, as we experienced. For each frequency a relationship between the average quarter-wavelength velocity and expected amplification was defined in the log space using a weighted, orthogonal, linear least-squares regression over the station samples (Krystek and Anton, 2008). The regression facilitates the estimation of amplification for average velocity classes that are not covered by direct measurement (Fig. 6). The weighting scheme used allows the consideration of uncertainty in both parameters. Finally, for each relationship, confidence bounds are computed from the orthogonal standard deviation of the residuals.

For most of the frequencies, a clear linear correlation is observed. However, in some cases (e.g., 3–5 Hz) the correlation between low-velocity values (300 to 750 m/s) and amplification is less well defined. This may be due to a lack of resolution in the MASW measurements at greater depths. More likely, however, is that this is due to the irregular shape of the amplification functions at these frequencies; typically a resonance minimum is present (Fig. 5, e.g., stations BOURR at 5 Hz and WIMIS at 3 Hz) or a resonance maximum (e.g., station WILA at 5 Hz). Consequently, the correlation functions exhibit some scatter with respect to the empirical amplification (Fig. 7).

For each analyzed frequency relation, it was assumed that the reference condition's average velocity corresponds to amplification equal to unity in the regression. Consequently,

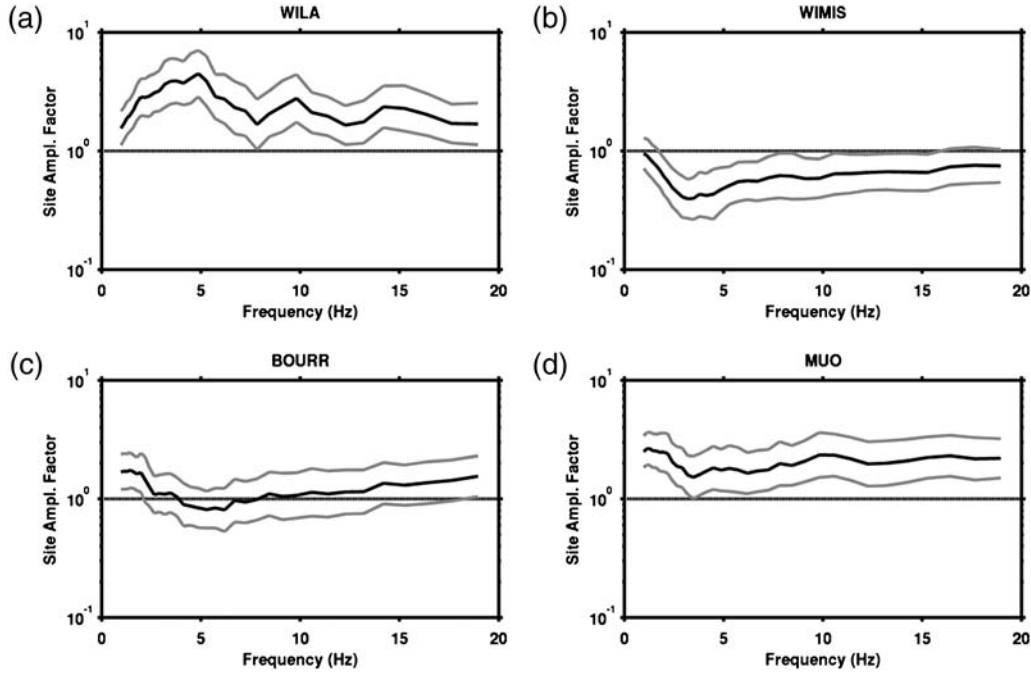


**Figure 5.** (a–d) All are examples of the amplification function from spectral modeling. The black line shows the mean amplification, and the gray lines indicate the standard deviation. The amplification functions are referenced to an unknown site condition that is later defined as part of this study.

we can reconstruct a quarter-wavelength representation of the whole reference profile (as  $\bar{V}_S^{\text{QWL}}(f)$  and  $\bar{z}^{\text{QWL}}(f)$ ), extracting the ensemble of selected quarter-wavelength velocities that show null amplification over the range of different frequencies (Fig. 8). The resulting profile shows a clear trend, with average velocity of about 1000 m/s at the surface progressively increasing with increasing depth.

### Inverting for a Gradient Model

The previous analysis provided a reference quarter-wavelength velocity profile that was defined to have null average amplification of the sites relative to the reference. However, this profile cannot be directly used for computing the site-to-reference  $SH$  amplification function. Reconstructing the standard  $V_S$  velocity profile from its corresponding quarter-wavelength representation is achieved by means of a global optimization procedure. A simplified gradient velocity profile is used for the inversion. The proposed equation is exponential, but differs with respect to other gradient models in literature (e.g., Faust, 1951) in the use of the coefficients to define the gradient bending (curvature parameters  $a$  and  $b$ ) along with the possibility of including *a priori* information about the lower bedrock velocity:

$$V_S(z) = (V_{S_{\max}} - V_{S_{\min}}) \left[ 1 - a^{\left(\frac{z_{\text{top}} - z}{b}\right)} \right] + V_{S_{\min}}. \quad (19)$$

This last point is fundamental because no information about depths greater than about few hundreds meters (here roughly higher than 200 ~ 250 m) can be extrapolated from the

measurements. Consequently, a velocity constraint must be defined. In our approach the lower bedrock velocity ( $V_{S_{\max}}$ ) is based on the estimation of the  $V_S$  velocity at 4000 m obtained from  $P$ -wave crustal travel-time tomography (Husen *et al.*, 2003), assuming a  $V_P/V_S$  ratio of 1.73 (or Poisson's ratio 0.25 for the upper crust). The estimated value is around  $V_{S_{\max}} = 3200$  m/s. The link depth has been determined according to the resolution limits of tomographic models at shallower depths, which typically provide unreliable estimations coarsely above 2000 m in depth. Using this reference bedrock velocity as the lower constraint for the profile, the inversion routine fits the best gradient model with curvature ( $a$  and  $b$ ) and upper-link velocity ( $V_{S_{\min}}$  estimated at the depth  $z_{\text{top}}$ ) to the quarter-wavelength data obtained previously.

Inverting a quarter-wavelength profile consists of a double-data-set-fitting problem. The quarter-wavelength velocity and depth ( $\bar{V}_S^{\text{QWL}}(f)$  and  $\bar{z}_f^{\text{QWL}}(f)$ ) curves of the reference have to be fit simultaneously. A cost function is calculated over the frequency range from 1 to 15 Hz using L2 norm assuming lognormal statistics:

$$M_{V_S} = \sum_{f=1}^{15 \text{ Hz}} \left[ \frac{\log(\bar{V}_{S_f}^{\text{QWL,Obs}}) - \log(\bar{V}_{S_f}^{\text{QWL,Syn}})}{\sigma(\bar{V}_{S_f}^{\text{QWL,Obs}})} \right]^2, \quad (20)$$

$$M_z = \sum_{f=1}^{15 \text{ Hz}} \left[ \frac{\log(\bar{z}_f^{\text{QWL,Obs}}) - \log(\bar{z}_f^{\text{QWL,Syn}})}{\sigma(\bar{z}_f^{\text{QWL,Obs}})} \right]^2, \quad (21)$$

where Obs indicates the reference profile derived from the  $\bar{V}_S^{\text{QWL}}(f)$ -amplification correlations at discrete frequencies

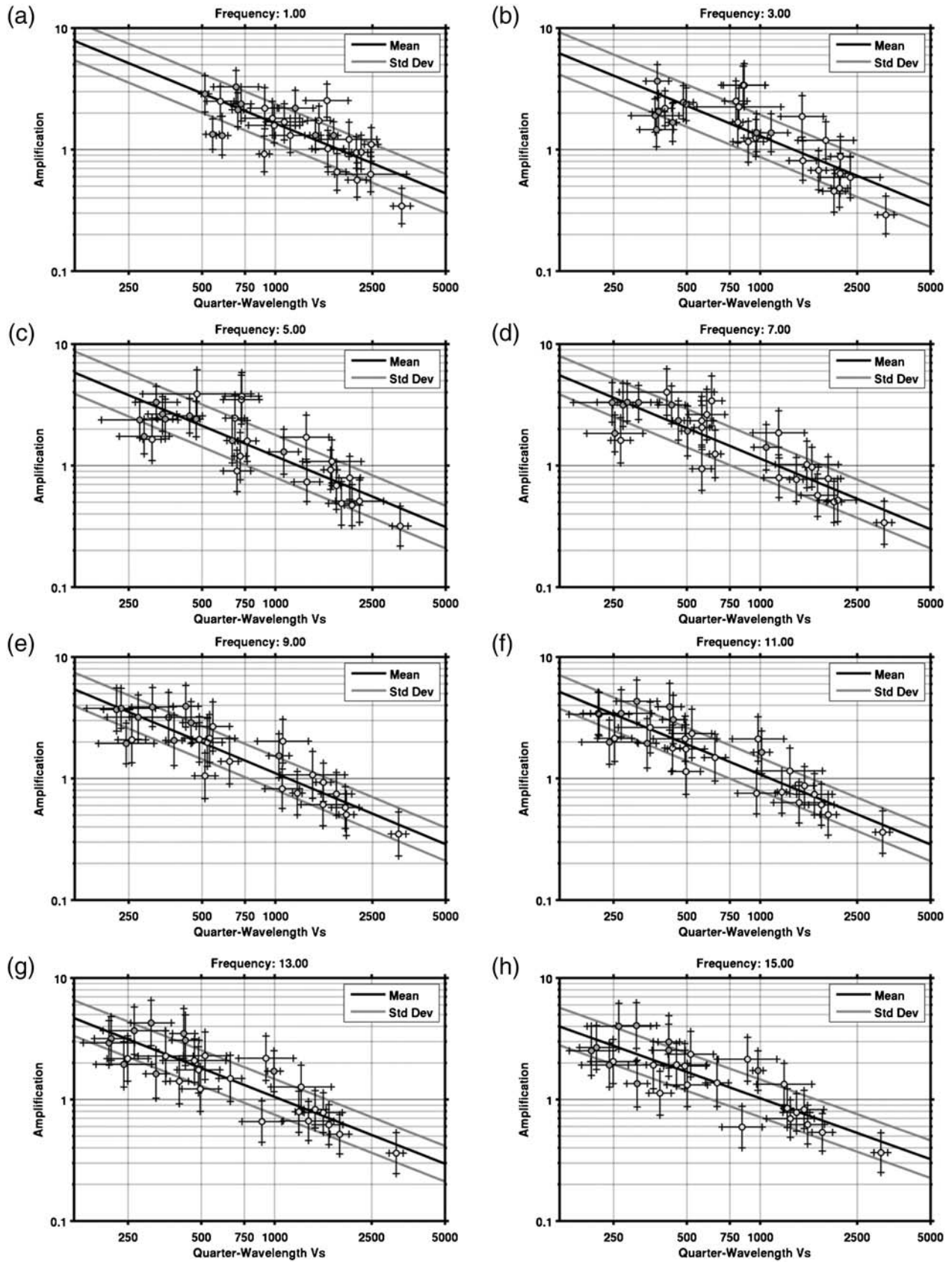


**Figure 6.** (a–h) All show the correlation between quarter-wavelength average velocities (MASW with dots in light gray, ambient noise in dark gray) and amplification factors from spectral modeling of earthquake spectra. A linear least-squares regression is applied in log–log scale to estimate parameter correlation.

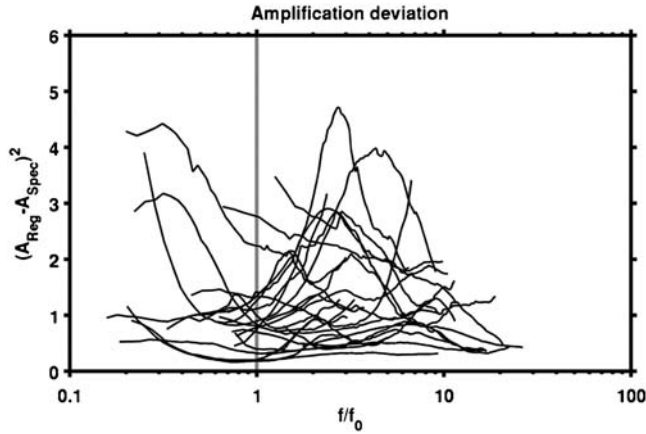


**Figure 7.** Quadratic residuals (in log-statistics) from the comparison of the empirical amplification functions and the mean amplification from the regression with quarter-wavelength average velocities. For each curve, the frequency axis has been normalized to the  $SH$  fundamental frequency of resonance of the site ( $f_0$ ). It is clear that deviations generally increase before and after the  $f_0$  value ( $f/f_0 = 1$ ).

$f$ , and Syn the inverted profile. Uncertainties on both parameters are taken into account. A global misfit is then computed as a simple sum:

$$M_{\text{Global}} = M_{V_s} + M_z. \quad (22)$$

The results of the optimization are shown in Figure 9, with best fit for the profile parameters  $a = 1.30$ ,  $b = 78.16$ , and  $V_{s_{\text{min}}} = 1000$  m/s. Some discrepancies between the data and model are apparent below 300 m. However, the deviation is within the error bounds of the input model.

## Comparison with Previous Reference Profiles

In Figure 10, the reference profile is presented together with shear-wave velocity profiles from  $P$ -wave regional tomography (Husen *et al.*, 2003) at three selected stations: HASLI, WEIN, and LLS. For the conversion, a  $P:S$  velocity ratio of 1.73 is used. The purpose of this comparison is to show how the proposed reference integrates and extends the tomographic profiles at shallow depths. As mentioned, profiles from crustal travel-time tomography have no resolution at shallower depths due to the lack of crossing ray paths in this region. Moreover, the spacing between grid nodes is generally insufficient to produce a sufficiently detailed representation of the structure in the upper layers. Unfortunately, shallower velocities have an important influence on the modification of the final ground motion. For this reason, the sole use of tomographic profiles should be avoided in the calibration of ground-motion prediction equations. However, as in the present work, the velocity values from these profiles at greater depths are useful for the calibration of the reference profile because no reliable constraint can be obtained at these depths from direct, low-cost measurements.

The reference profile computed using the quarter-wavelength approximation has also been compared with previous reference velocity profiles from ambient noise recordings constrained by borehole measurements (Takahashi and Suzuki, 2001) and an interpretation of reflection and refraction studies (Campus and Fäh, 1997; Fäh *et al.*, 2003) in selected regions of Switzerland (Fig. 11). It should be noted that, within the group, the models Zentralschweiz, Innerschweiz 01, and Innerschweiz 02 are solely representative of the Alpine and pre-Alpine regions, while only Mittelland

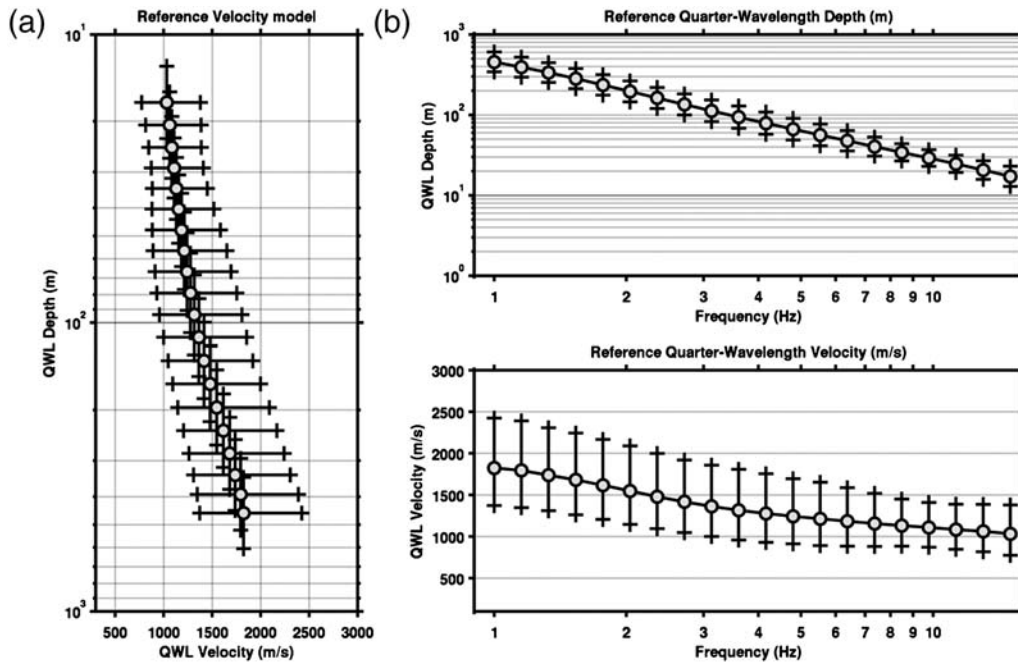


**Figure 8.** Quarter-wavelength representation of the reference velocity profile. (a) The profile is presented with average velocity versus depth; (b) the frequency dependency of the quarter-wavelength parameters is emphasized.

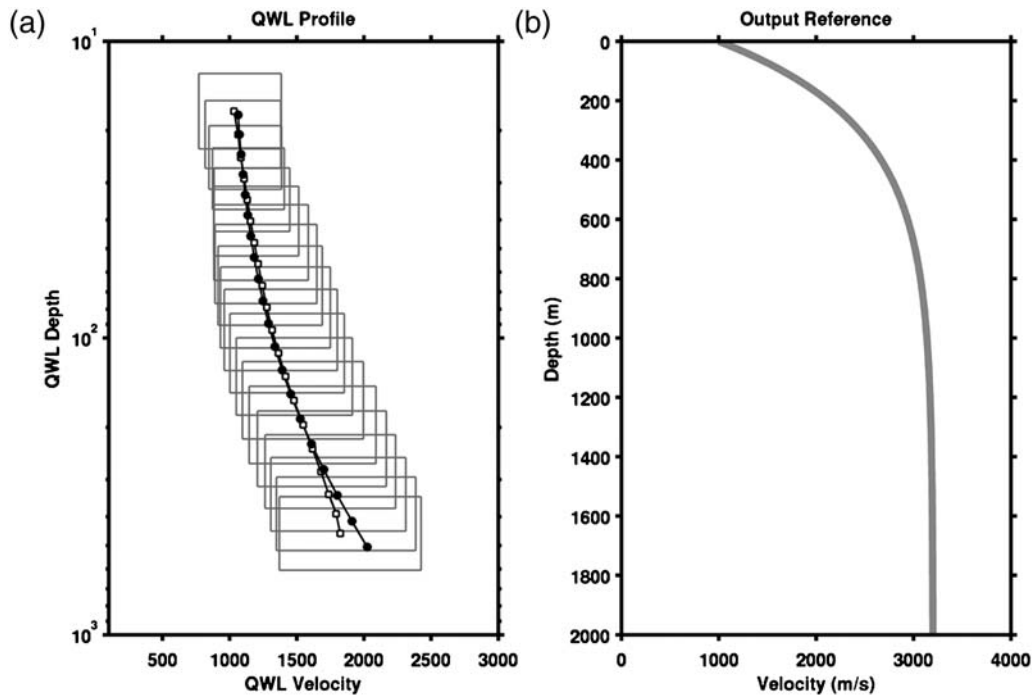


**Figure 9.** Reconstruction of the reference velocity profile from its quarter-wavelength representation: (a) is the fit between the observed (white squares) and the inverted (black dots) profiles, and (b) is the corresponding best-fitting model in gradient form.

and Basel (named Average Model in Fäh *et al.*, 2003) describe the Swiss Alpine Foreland. The proposed reference is generally in agreement with the measurements. It generally matches the average trend of the whole set of profiles. Some discrepancies are present at very shallow depths, where the velocities in our model (about 1000 m/s) are slightly higher than the average from ambient noise recordings (around 600 m/s), but lower than those from the interpretation of seismic surveys (greater than 2000 m/s in some models). This can be explained by considering that ambient noise techniques are generally sensitive to the uppermost low-velocity layers such as soft sediment cover or weathered rock soils, while seismic surveys tend to be more insensitive to the uppermost structure. Ambient noise profiles are also subject to a progressive lack in resolution with increasing depth. This might result in a biased estimation of the seismic velocity at greater depths, especially when very soft sediments are present at the surface. Apart from the fact that the profiles are all located in the Northern Swiss Foreland, such smoothing effects might also explain the discrepancies in gradient slopes between the presented data sets. Note, however, that the proposed reference profile has to be considered as the solution that explains the data in terms of amplification. It is solely representative of a pure theoretical rock condition, averaged over the different sites used to define the predicted ground motion. Consequently, it might not necessarily match an existing profile from a specific area.

The retrieved reference was compared with two generic rock velocity models proposed by Boore and Joyner (1997) for North America. These profiles are often used in practice

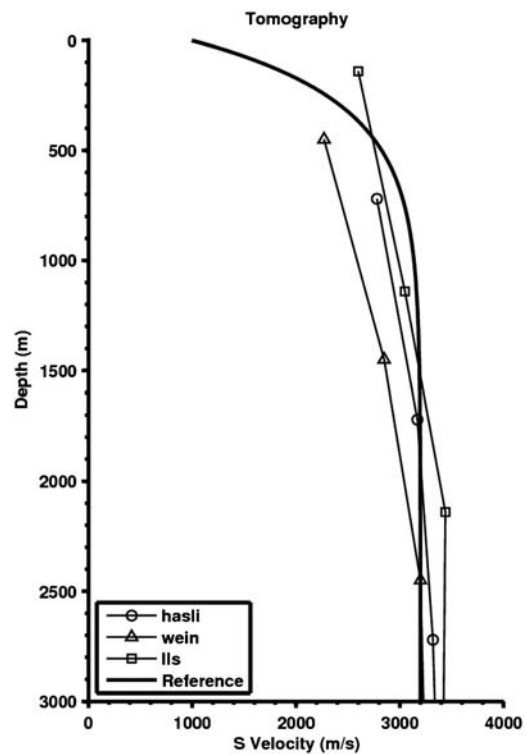


**Figure 10.** Comparison between profiles from converted  $P$ -wave travel-time tomography in selected regions of Switzerland with the proposed reference. Tomographic profiles have been used to constrain the bedrock velocity of the reference at a large depths during the inversion.

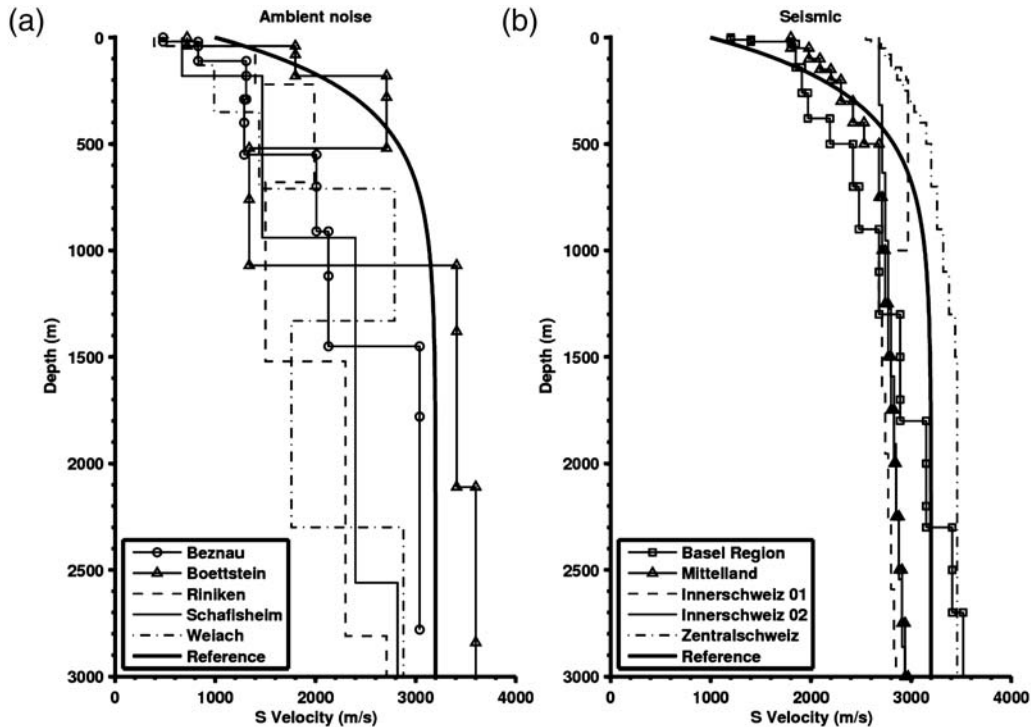


**Figure 11.** Comparison of the proposed reference velocity profile with previous references from independent studies in Switzerland: (a) profiles from array processing of ambient noise (Takahashi and Suzuki, 2001) and (b) interpretation of seismic refraction and reflection studies (Campus and Fäh, 1997; Fäh *et al.*, 2003).

as reference for the GMPs and are based on two different assumptions. The first profile (Fig. 12, curve A) was established to represent the average condition for rock sites of engineering significance, while the second (Fig. 12, curve B) is specifically representative of very hard-rock sites, such as those where glacial erosion removed the uppermost weathered part. If compared with the proposed reference, some differences are noticeable. In particular, the presented reference profile shows considerably higher velocity at shallow depths ( $V_{S30} = 1106$  m/s) than profile A ( $V_{S30} = 618$  m/s), but remarkably lower velocity than profile B ( $V_{S30} = 2880$  m/s). This intermediate condition might be explained by the differences in lithology and dynamic setting between the study areas. Differences in the gradient slope are also evident. However, this is probably induced by the different forms of the equations used to model the profiles and, as mentioned before, by the velocity constraints imposed at depth.

#### Reference Amplification Model

From the inverted velocity profile, we computed amplification functions. Two distinct approaches were followed. First, we computed the 1D *SH*-wave transfer function for vertical wave propagation following the Knopoff layer-matrix formulation (Knopoff, 1964). Unfortunately, we obtained no reliable estimation of density from direct measurements (dispersion curve inversions have virtually no

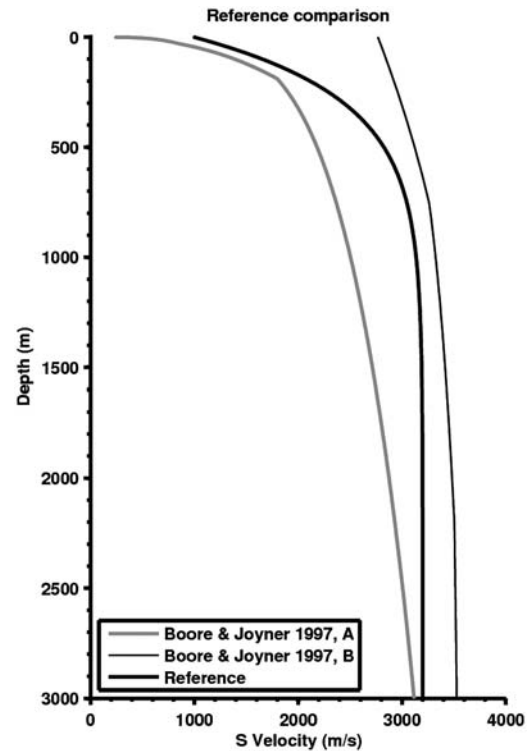


**Figure 12.** Comparison between the reference *S*-wave velocity profile proposed for Switzerland with the results from Boore and Joyner (1997) for North America. Profile A is representative of a generic rock condition, while in B the reference is computed for very hard-rock sites.

resolution on this parameter). Consequently, it was not possible to reconstruct and use any reference density profile with the proposed method. For this reason, a constant value of  $2500 \text{ kg/m}^3$  has been established for the whole reference profile. Such approximation is acceptable if no large density variations are expected. In fact, the relative amplification is weakly affected by this parameter. As an example, a density contrast between  $2100 \text{ kg/m}^3$  (at the top) and  $2900 \text{ kg/m}^3$  (at the bottom) will affect the maximum amplification, with respect to the proposed constant model, by a factor 1.16 only. As the crustal reference, a homogeneous half-space with a constant shear-wave velocity of  $3200 \text{ m/s}$  and a density of  $2500 \text{ kg/m}^3$  is assumed. The model is purely elastic, and no attenuation has been considered, as this can be applied separately. Next, we computed the spectral amplification from quarter-wavelength approximation, as described in [Boore and Joyner \(1997\)](#). Following this approach, we give amplification as the square root of the ratio between the average seismic impedance at the corresponding quarter-wavelength depth and the impedance of the reference (equation 6). As in the previous case, a constant  $S$ -velocity ( $V_S^C$ ) of  $3200 \text{ m/s}$  and density ( $\rho^C$ ) of  $2500 \text{ kg/m}^3$  were assumed as a reference.

When compared, the amplification functions from the two approaches look similar and partially overlap (Fig. 13). This is expected in the case of a simplified gradient model with no large contrasts of impedance at depth, which would, if present, give rise to the characteristic resonance peaks in the  $SH$ -transfer function representation. However, some differences are present around  $1 \text{ Hz}$ , where the  $SH$ -transfer function is higher than that one computed from simple impedance ratios. In order to be conservative, we therefore decided to adopt the  $SH$ -wave model as a more reliable representation of the reference amplification. In more detail, the amplification function is a ramp function, which asymptotically converges to a stable value of about 1.78 at high

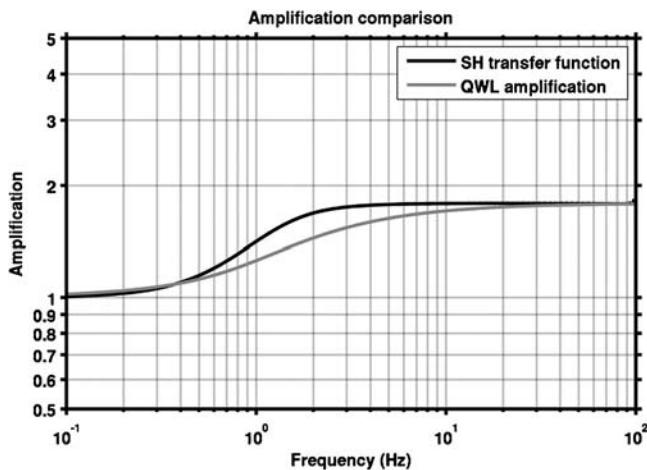


**Figure 13.** Absolute value of the 1D  $SH$ -transfer function and the amplification from the quarter-wavelength method computed for the proposed reference rock profile, assuming a common constant crustal reference of  $3200 \text{ m/s}$ . Some differences in the amplification level are noticeable in a frequency band between  $0.5$  and  $10 \text{ Hz}$ .

frequencies (the plateau level). The bending of the curve is controlled by the curvature of the inverted gradient profile. The stronger variation of amplification occurs over a range between  $0.5$  and  $10 \text{ Hz}$ .

In comparison to the amplification functions of reference profiles derived from the interpretation of seismic refraction and reflection surveys of Figure 11, the  $SH$ -wave amplification of the proposed reference shows some differences (Fig. 14). The average level of amplification is generally higher for frequencies greater than  $1 \text{ Hz}$ . The Basel profile is the most similar in terms of amplification, especially in the plateau region. Conversely, InnerSchweiz and ZentralSchweiz profiles are models representative of the Alpine and pre-Alpine areas and give rise to considerably lower amplification. As previously described, this is induced by higher near-surface velocities in the Alpine region. We think that such high velocities are not representative of the average reference condition of Switzerland.

Finally, we compared the amplification function of the reference with those from the two rock profiles proposed for North America by [Boore and Joyner \(1997, in Figure 12\)](#). As in the previous cases, no attenuation was considered for the computation. Specifically, the amplification function for the generic rock site condition of North America (Fig. 15, curve A) is always higher than the one computed for the proposed reference. Differences are consistent especially at high frequencies ( $> 20 \text{ Hz}$ ), where profile A shows amplification up to two times higher than the Swiss reference. This is clearly induced by the choice of very low velocities ( $< 600 \text{ m/s}$ ) at shallow depths, which are not applicable for Switzerland. On the other hand, profile B has amplification nearly flat and close to 1 for all frequencies. This is expected for very hard-rock conditions, but might be inappropriate as use for

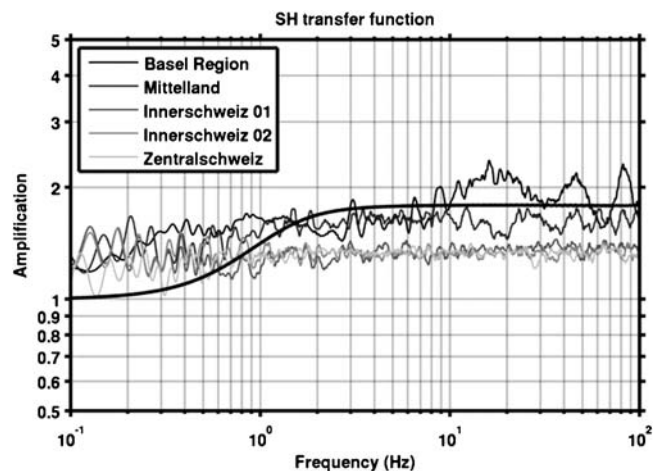


**Figure 14.** Comparison between  $SH$ -amplification function of the reference profile (thick line) and those from the interpretation of seismic refraction and reflection studies in Switzerland. The proposed amplification model is representative of the Swiss Foreland and is therefore more consistent with the amplification models for the Basel region and the Mittelland.

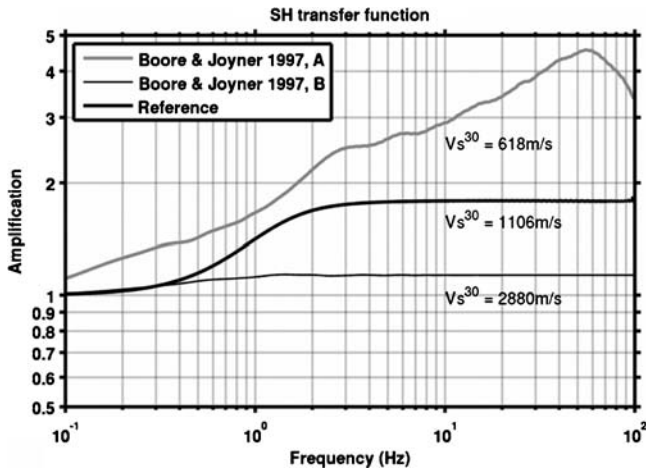


**Figure 15.** Amplification function of the proposed reference compared to the results from Boore and Joyner (1997) for North America. Profile A gives the amplification for a generic rock site, while B gives the amplification for very hard-rock conditions.  $V_{s30}$  estimations for each profile are also presented to emphasize the differences in average amplification, especially at high frequencies.

a standard reference, where the average effect of weathered and fractured rock conditions should be taken into account.

The maximum level of amplification of the reference transfer function is controlled by the velocity contrast between the uppermost part of the profile and the crustal basement. However, because the velocities at shallow depths are constrained by direct measurement, the amplification at high frequencies (the plateau region) will be strictly conditioned by the choice of the lowermost velocity constraint. Clearly, some uncertainties are present in the definition of both parameters, and this may be reflected in the average level of amplification. We tested the variability in the amplitude of the plateau by changing the upper and lower velocity links of the reference profile (Fig. 16). The upper velocity was allowed to vary between 940 and 1060 m/s, and the lower between 3000 and 3400 m/s. This led to variations in the amplification factors between 1.68 and 1.89, corresponding

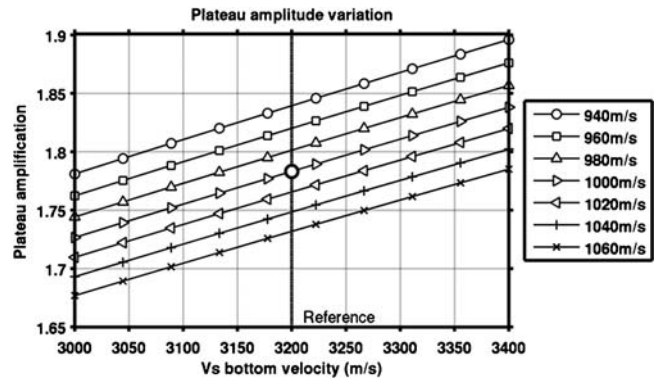


**Figure 16.** Variations in the amplitude of the plateau region of the reference amplification function induced by different bottom (on x axis) and upper-layer velocities (marked curves). The actual reference is marked with a circle at the corresponding bottom  $V_s$  velocity of 3200 m/s.

to an uncertainty of less than 10% in the proposed reference value.

### Back-Computation of the Amplification Functions

Coefficients from the correlation between quarter-wavelength average velocities and empirical amplification from spectral modeling can be used to reconstruct the frequency-dependent amplification function for sites with a quarter-wavelength velocity profile (Table 1). To assess the consistency of the results, we compare the reconstructed amplification with the empirical and theoretical amplification functions for those sites that have been surveyed with passive array analysis. The choice of using this set of locations is driven by the fact that ambient noise processing provides higher resolution of the velocity structure at depth. A more accurate theoretical amplification function can then be modeled.

A good agreement is generally present when comparing the reconstructed amplification functions with those from the empirical spectral modeling approach. Amplifications reconstructed from the quarter-wavelength velocity (abbreviated

**Table 1**  
Mean Amplifications Computed from the Regression between Quarter-Wavelength Velocities and Amplification Factors from Spectral Modeling of Earthquakes

Quarter-Wavelength S-Velocity	Frequency (Hz)											
	1	2	3	4	5	6	7	8	9	10	15	
200	6.18	5.05	4.88	4.66	4.57	4.36	4.36	4.34	4.24	4.24	3.24	
300	4.42	3.67	3.49	3.33	3.26	3.12	3.11	3.09	3.02	3.01	2.42	
400	3.49	2.92	2.75	2.62	2.56	2.45	2.45	2.42	2.38	2.37	1.97	
500	2.9	2.45	2.29	2.18	2.13	2.04	2.03	2.01	1.97	1.96	1.68	
600	2.5	2.12	1.97	1.88	1.83	1.75	1.75	1.72	1.69	1.68	1.47	
800	1.97	1.69	1.56	1.48	1.44	1.38	1.37	1.35	1.33	1.32	1.2	
1000	1.64	1.42	1.29	1.23	1.19	1.15	1.14	1.12	1.1	1.1	1.02	
1250	1.37	1.19	1.08	1.02	0.99	0.95	0.95	0.93	0.92	0.91	0.87	
1500	1.17	1.03	0.93	0.88	0.85	0.82	0.81	0.8	0.79	0.78	0.76	
2000	0.93	0.82	0.73	0.69	0.67	0.65	0.64	0.62	0.62	0.61	0.62	
2500	0.77	0.69	0.61	0.58	0.56	0.54	0.53	0.52	0.51	0.51	0.53	
3000	0.66	0.59	0.52	0.5	0.48	0.46	0.46	0.44	0.44	0.44	0.46	

QWL in the equations and figures) amplification correlations are incapable of reproducing the small features typical of an empirical function, such as peaks and troughs (e.g., SMZW, Fig. 17c), at sites with unconsolidated sediments. The trend is nevertheless clearly preserved. Sometimes, an offset is exhibited between the two functions (e.g., SULZ, Fig. 17b). Such a discrepancy, however, can be easily explained by the fact that the linear regression produces a common least-square solution, but the local amplification at a site can be locally deviated from the retrieved average. The local amplification, moreover, might be influenced by a velocity jump at depths not resolved by the  $S$ -wave measurements.

As mentioned, amplification factors reconstructed from the correlation have also been compared with theoretical 1D amplification functions, using  $SH$ -transfer-function formalism. For the computation of amplification using  $SH$ -wave site response, we used the proposed reference profile. The comparison shows good agreement between the amplification curves for sites with larger  $V_{S30}$ . Some discrepancies between the empirical amplification and the reconstructed

amplification are noticeable (Fig. 17c), but most times the curve falls within the error bounds of the regression.

## Summary and Conclusions

We proposed a new method to estimate the reference shear-wave velocity profile to be used in probabilistic seismic-hazard assessment. The procedure is based on the comparison between *in situ* direct measurements and amplification factors from earthquake spectral modeling. The quarter-wavelength approximation was used to isolate average velocities and compare them to the frequency-dependent amplification.

The reference profile that we retrieved consists of a simplified gradient model with monotonically increasing velocity from about 1000 m/s to 3200 m/s. Our result is in agreement with studies conducted using different approaches, such as measurements taken using ambient noise recordings constrained by borehole measurements and interpretation of seismic reflection and refraction techniques. From this profile,

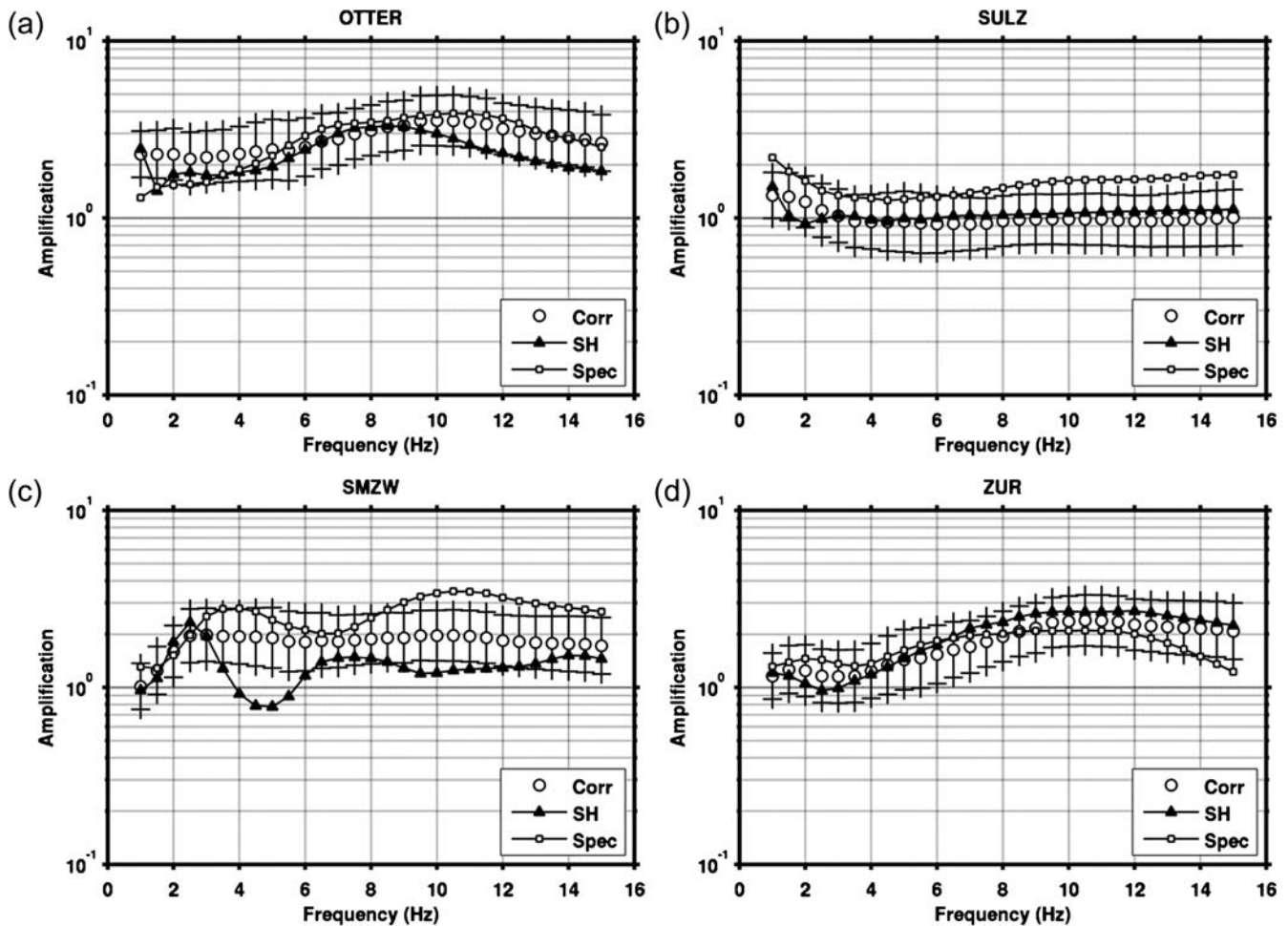


**Figure 17.** Generic amplification functions (Corr) can be reconstructed from the coefficients of the correlations between average quarter-wavelength velocities and empirical amplifications at all stations. The empirical amplification for the specific station is also given (Spec). The result is consistent with the modeled site-specific amplification using the  $SH$ -transfer function ( $SH$ ), especially for the sites with higher  $S$ -wave velocity at the surface. (a)  $V_{S30} = 418$  m/s; (b)  $V_{S30} = 1034$  m/s; (c)  $V_{S30} = 483$  m/s; (d)  $V_{S30} = 635$  m/s.

we computed the *SH*-wave transfer function, assuming a constant reference of 3200 m/s for use in a stochastic model.

The amplification functions derived from spectral modeling of earthquakes were shown to be generally consistent with the results from the 1D *SH*-wave transfer function for stiff soils to rock sites. However, these functions also included small-scale local features that were not possible to model with a simplified approach. We showed that amplification functions for specific sites in Switzerland with a quarter-wavelength velocity profile could be reconstructed using the correlation relations defined in this study. The general trend of the amplification functions was recovered when compared to those derived from the *SH*-transfer function for real sites. The reconstructed amplification relations provide a useful alternative method for assessing the site amplification in the absence of earthquake recordings without the necessity of using *SH*-wave modeling. However, there is space for improvement when the influence of very strong velocity contrasts is included.

The uncertainties in the resulting amplification function have been taken into account. These are mostly induced by the limited extension of our measurement data set. We are confident that including additional data will improve the statistics. To do this, we plan to perform additional measurements at seismological station locations for which amplification functions are available from spectral modeling. Moreover, other than active seismic measurements, a progressively increasing number of results from ongoing and planned ambient noise recording measurements will be added to the data set. This will increase resolution especially at greater depths. Furthermore, once a larger data set is available, we suggest developing different reference profiles for the main geological domains of Switzerland. This will include the Molasse Basin, the Alpine (including the Prealps), and the Jura regions. It is important to underline that these domains show considerable differences from the tectonic and lithological point of view, and it is more appropriate to treat them separately in the context of probabilistic seismic-hazard assessment.

### Data and Resources

Velocity profiles from ambient noise and MASW analysis are part of the site characterization database of the Swiss Seismological Service (SED). The database will be released to the public in December 2010. Restricted access, however, can be granted before this date upon direct request to donat-faeh@sed.ethz.ch. The 585 earthquake events used for site-specific amplification computation have been extracted from the recording database of SED. These data are available for the public through AutoDRM (<http://www.seismo.ethz.ch/prod/autodrm>, last accessed May 2010). Other data are available for the public from sources referenced in the paper.

### Acknowledgments

This research was supported by the project HAZARD 2010 (S.N.F. No. 200021-112284) and also by the projects PRP (PEGASOS Refinement

Project) and SHARE (Seismic-Hazard Harmonization in Europe). We acknowledge GeoExpert AG who performed the MASW surveys. We also acknowledge John Douglas, an anonymous reviewer, and Associate Editor Stefano Parolai for their helpful comments and suggestions. A final thanks goes to Stefan Fritsche and Gabriela Gassner-Stamm for their help in compiling the measurement database.

### References

- Abbiss, C. P. (1989). Seismic amplification—Mexico City, *Earthquake Eng. Struct. Dynam.* **18**, 79–88.
- Aki, K. (1993). Local site effects on weak and strong motion, *Tectonophysics* **218**, 93–111.
- Akkar, S., and J. J. Bommer (2007). Prediction of elastic displacement response spectra in Europe and the Middle East, *Earthquake Eng. Struct. Dynamics* **36**, 1275–1301.
- Anderson, J. G., and S. E. Hough (1984). A model for the shape of the Fourier amplitude spectrum of acceleration at high frequencies, *Bull. Seismol. Soc. Am.* **74**, 1969–1993.
- Atkinson, G. M., and D. M. Boore (2006). Earthquake ground-motion prediction equations for eastern North America, *Bull. Seismol. Soc. Am.* **96**, 2181–2205.
- Atkinson, G., and R. Mereu (1992). The shape of ground motion attenuation curves in southeastern Canada, *Bull. Seismol. Soc. Am.* **82**, 2014–2031.
- Baer, M., N. Deichmann, J. Braunmiller, J. Clinton, S. D. Husen, D. Giardini, P. Kästli, U. Kradolfer, and S. Wiemer (2007). Earthquakes in Switzerland and surrounding regions during 2006, *Eclogae Geol. Helv.* **100**, 3, 517–528.
- Bard, P. Y., M. Campillo, F. J. Chávez-García, and F. J. Sánchez-Sesma (1988). Strong ground motion in Mexico City during the great Michoacan earthquake. Part B: A theoretical investigation of large- and small-scale amplification effects, *Earthq. Spectra* **4**, 609–633.
- Bindi, D., S. Parolai, H. Grosser, C. Milkereit, and S. Karakisa (2006). Crustal attenuation characteristics in Northwestern Turkey in the range from 1 to 10 Hz, *Bull. Seismol. Soc. Am.* **96**, 200–214.
- Bonilla, L. F., J. H. Steidl, G. T. Lindley, A. G. Tumarkin, and R. J. Archuleta (1997). Site amplification in the San Fernando Valley, California: Variability of site-effect estimation using the *S*-wave, coda, and H/V methods, *Bull. Seismol. Soc. Am.* **87**, 710–730.
- Boore, D. M. (1983). Stochastic simulation of high-frequency ground motions based on seismological models of the radiated spectra, *Bull. Seismol. Soc. Am.* **73**, 1865–1894.
- Boore, D. M. (2003). Simulation of ground motion using the stochastic method, *Pure Appl. Geophys.* **160**, 3–4, 635–676.
- Boore, D. M., and W. B. Joyner (1997). Site amplifications for generic rock sites, *Bull. Seismol. Soc. Am.* **87**, 327–341.
- Borcherdt, R. D. (1970). Effects of local geology on ground motion near San Francisco Bay, *Bull. Seismol. Soc. Am.* **60**, 29–81.
- Borcherdt, R. D., and J. F. Gibbs (1976). Effects of local geological conditions in the San Francisco Bay region on ground motions and the intensities of the 1906 earthquake, *Bull. Seismol. Soc. Am.* **66**, 467–500.
- Brune, J. N. (1970). Tectonic stress and the spectra of seismic shear waves from earthquakes, *J. Geophys. Res.* **75**, 4997–5010.
- Brune, J. N. (1971). Correction: Tectonic stress and the spectra of seismic shear waves from earthquakes, *J. Geophys. Res.* **76**, 5002.
- BSSC, Building Seismic Safety Council (2003). The 2003 NEHRP Recommended provisions for new buildings and other structures, Part 1: Provisions (FEMA 450), [www.bssconline.org](http://www.bssconline.org).
- Campus, P., and D. Fäh (1997). Seismic monitoring of explosions: A method to extract information on the isotropic component of the seismic source, *J. Seism.* **1**, 205–218.
- Capon, J. (1969). High-resolution frequency-wavenumber spectrum analysis, *Proc. IEEE* **57**, 1408–1418.
- Castro, R. R., J. G. Anderson, and S. K. Singh (1990). Site response, attenuation and source spectra of *S* waves along the Guerrero, Mexico, subduction zone, *Bull. Seismol. Soc. Am.* **80**, 1481–1503.

- CEN, European Committee for Standardization (2004). Eurocode 8: Design of structures for earthquake resistance—Part 1: General rules, seismic actions and rules for buildings, *British Standard BS EN 1998-1:2004*: E, pp.219.
- Douglas, J., P. Gehl, L. F. Bonilla, O. Scotti, J. Regnier, A. M. Duval, and E. Bertrand (2009). Making the most of available site information for empirical ground-motion prediction, *Bull. Seismol. Soc. Am.* **99**, 3, 1502–1520.
- Drouet, S., S. Chevrot, F. Cotton, and A. Souriau (2008). Simultaneous inversion of source spectra, attenuation parameters, and site responses: Application to the data of the French accelerometric network, *Bull. Seismol. Soc. Am.* **98**, 1, 198–219.
- Drouet, S., F. Cotton, and P. Guéguen (2010).  $V_{S30}$ ,  $\kappa$ , regional attenuation and  $M_w$  from accelerograms: Application to magnitude 3 to 5 French earthquakes, *Geophys. J. Int.* **182**, 2, 880–898.
- Drouet, S., P. Triantafyllidis, A. Savvaidis, and N. Theodulidis (2008). Comparison of site-effects estimation methods using the Lefkas Greece 2003 earthquake aftershocks, *Bull. Seismol. Soc. Am.* **98**, no. 5, 2349–2363. doi [10.1785/0120080004](https://doi.org/10.1785/0120080004).
- Edwards, B., and A. Rietbrock (2009). A comparative study on attenuation and source-scaling relations in the Kanto, Tokai, and Chubu Regions of Japan, using data from Hi-Net and Kik-Net, *Bull. Seismol. Soc. Am.* **99**, doi [10.1785/0120080292](https://doi.org/10.1785/0120080292).
- Edwards, B., B. Allmann, D. Fäh, and V. Poggi (2009). Stochastic model for Switzerland, *Swiss Seismological Service Technical Report: SED/PRP/R/006/20091130*, for the *swissnuclear* PEGASOS Refinement Project.
- Edwards, B., A. Rietbrock, J. J. Bommer, and B. Baptie (2008). The acquisition of source, path and site effects from microearthquake recordings using  $Q$  tomography: Application to the United Kingdom, *Bull. Seismol. Soc. Am.* **98**, 1915–1935.
- Fäh, D., S. Fritsche, V. Poggi, G. Gassner-Stamm, P. Kästli, J. Burjanek, P. Zweifel, S. Barman, J. Clinton, L. Keller, P. Renault, and S. Heuberger (2009). Determination of site information for seismic stations in Switzerland, *Swiss Seismological Service Technical Report: SED/PRP/R/004/20090831*, for the *swissnuclear* PEGASOS Refinement Project.
- Fäh, D., F. Kind, and D. Giardini (2003). Inversion of local  $S$ -wave velocity structures from average  $H/V$  ratios, and their use for the estimation of site-effects, *J. Seism.* **7**, 449–467.
- Fäh, D., G. Stamm, and H. B. Havenith (2008). Analysis of three-component ambient vibration array measurements, *Geophys. J. Int.* **172**, 199–213.
- Faust, L. Y. (1951). Seismic velocity as a function of depth and geologic time, *Geophysics* **16**, 2, 192–206.
- GeoExpert AG (2009). Seismic shear wave velocity determination and hybrid seismic surveying at 20 SED stations in Switzerland, Summary report for the *swissnuclear* PEGASOS Refinement Project.
- Hanks, T. C., and R. K. McGuire (1981). The character of high frequency strong ground motion, *Bull. Seismol. Soc. Am.*, **71**, 2071–2095.
- Havenith, H. B., D. Fäh, U. Pollom, and A. Roulle (2007).  $S$ -wave velocity measurements applied to the seismic microzonation of Basel, Upper Rhine Graben, *Geophys. J. Int.* **170**, 346–358.
- Husen, S., E. Kissling, N. Deichmann, S. Wiemer, D. Giardini, and M. Baer (2003). Probabilistic earthquake location in complex three-dimensional velocity models: Application to Switzerland, *J. Geophys. Res.* **108**, B2, doi [10.1029/2002JB001778](https://doi.org/10.1029/2002JB001778).
- Ide, S., G. C. Beroza, S. G. Prejean, and W. L. Ellsworth (2003). Apparent break in earthquake scaling due to path and site effects on deep borehole recordings, *J. Geophys. Res.* **108**, B5, 2271, doi [10.1029/2001JB001617](https://doi.org/10.1029/2001JB001617).
- Joyner, W. B., R. E. Warrick, and T. E. Fumal (1981). The effect of Quaternary alluvium on strong ground motion in the Coyote Lake, California, earthquake of 1979, *Bull. Seismol. Soc. Am.* **71**, 1333–1349.
- Kawase, H. (2006). Site effects on strong ground motions, *International Handbook of Earthquake and Engineering Seismology, Part B*, W. H. K. Lee and H. Kanamori (Editors), Academic Press, London, 1013–1030.
- Knopoff, L. (1964). A matrix method for elastic wave problems, *Bull. Seismol. Soc. Am.* **54**, 431.
- Krystek, M., and M. Anton (2008). A weighted total least-squares algorithm for fitting a straight line, *Meas. Sci. Tech.* **18**, 3438–3442.
- Lees, J. M., and J. Park (1995). Multiple-taper spectral analysis: A stand-alone C-subroutine, *Comp. Geosciences* **21**, 199–236.
- Park, C. B., R. D. Miller, and J. Xia (1999). Multichannel analysis of surface waves, *Geophysics* **64**, 800–808.
- Park, J., C. R. Lindberg, and F. L. Vernon (1987). Multitaper spectral analysis of high frequency seismograms, *J. Geophys. Res.* **92**, 12675–12684.
- Parolai, S., D. Bindi, M. Baumbach, H. Grosser, C. Milkereit, S. Karakisa, and S. Zümbül (2004). Comparison of different site response estimation techniques using aftershocks of the 1999 Izmit earthquake, *Bull. Seismol. Soc. Am.* **94**, 1096–1108.
- Poggi, V., and D. Fäh (2009). Estimating Rayleigh wave particle motion from three-component array analysis of ambient vibrations, *Geophys. J. Int.* **180**, 1, 251–267.
- Pozo, R. (2004). Template Numerical Toolkit, <http://math.nist.gov/tnt/> (last accessed May 2009).
- Pratt, T. L., T. M. Brocher, C. S. Weaver, K. C. Miller, A. M. Tréhu, K. C. Creager, R. S. Crosson, and C. M. Snelson (2003). Amplification of seismic waves by the Seattle basin, northwestern U.S., *Bull. Seismol. Soc. Am.* **93**, 533–545.
- Press, W. H., S. A. Teukolsky, W. T. Vetterling, and B. P. Flannery (1997). *Numerical Recipes in C: The Art of Scientific Computing Second Edition*, Cambridge University Press, New York 278–281, 288–290, 417–424, 515–518.
- Randal, M. J. (1973). The spectral theory of seismic sources, *Bull. Seismol. Soc. Am.* **63**, 1133–1144.
- Renault, P., S. Heuberger, and N. A. Abrahamson (2010). PEGASOS refinement project: An improved PSHA for Swiss nuclear power plants, in *Proc. Fourteenth ECEE—European Conference of Earthquake Engineering*, Ohrid, Republic of Macedonia, Paper ID 991.
- Rietbrock, A. (2001).  $P$  wave attenuation structure in the fault area of the 1995 Kobe earthquake, *J. Geophys. Res.* **106**, 4141–4154.
- Roesset, J. M. (1970). Fundamentals of soil amplification, in *Seismic Design for Nuclear Power Plants*, R. J. Hansen (Editor), M. I. T. Press, Cambridge, Massachusetts, 183–244.
- Romero, S. M., and G. J. Rix (2001). Ground motion amplification of soils in the upper Mississippi embayment, *Rept. No. GIT-CEE/GEO-01-1*, Georgia Institute of Technology, Atlanta, Georgia.
- Scherbaum, F. (1990). Combined inversion for the three-dimensional  $Q$  structure and source parameters using microearthquake spectra, *J. Geophys. Res.* **95**, 12,423–12,438.
- Steidl, J. H., A. G. Tumarkin, and R. J. Archuleta (1996). What is a reference site?, *Bull. Seismol. Soc. Am.* **86**, 1733–1748.
- Yamanaka, H., M. Takemura, H. Ishida, and M. Niwa (1994). Characteristics of long-period microtremors and their applicability in exploration of deep sedimentary layers, *Bull. Seismol. Soc. Am.* **84**, 1831–1841.
- Yu, J., and J. Haines (2003). The choice of reference sites for seismic ground motion amplification analyses: Case study at Parkway, New Zealand, *Bull. Seismol. Soc. Am.* **93**, 713–723.
- Takahashi, T., and H. Suzuki (2001). A study on technical methodologies underpinning site selection process for geological disposal, A study on site screening system for geological disposal. Microtremor measurements, Radioactive Waste Management Center (RWNC), *Nagra Project Report 01–28*.

Swiss Seismological Service  
ETH Zürich  
Switzerland  
poggi@sed.ethz.ch